Este artículo es una visión general sobre el conocimiento de la cinética de disolución y precipitación de minerales adquirido en los últimos veinte años a partir de los estudios en que he participado.

This paper is an overview of the acquired knowledge on the mineral dissolution/precipitation kinetics over the last twenty years from the studies I have participated.

Mineral Dissolution and Precipitation Kinetics: Macroscopic, Microscopic and Nanoscopic Techniques

/ JORDI CAMA

Institute of Environmental Assessment and Water Research (IDAEA), CSIC, Jordi Girona 18, Barcelona 08034, Catalonia

INTRODUCTION

In this communication I comment on the studies in which I participated in the last two decades, covering the science of mineral dissolution/precipitation kinetics. The objective is to give a brief overview of the acquired knowledge about kinetics of complex processes, emphasizing on the various experimental approaches and methodologies utilized for this investigation. Over these 20 years our concerns with environmental contamination and remediation have leaded us to advance in the kinetics of water-rock interaction. We have centered our investigation in geochemical processes originated from four sources of anthropogenic contamination: *(1)* nuclear waste, *(2)* acid mine drainage (AMD), *(3)* groundwater (de)nitrification and *(4)* atmospheric accumulation/geological sequestration of CO_2. A common necessity in the management of these phenomena is the quantitative treatment of the geochemical evolution in the respective environments.

On the one hand, enhancement of the understanding of the mechanisms involving fluid flow and reactions with mineral surfaces requires incorporation of macroscopic to nanoscopic techniques in our studies. We have aimed at characterizing and quantifying the complex processes at the very low spatial scale. On the other hand, to predict the geochemical evolution in natural and artificial environments incorporation of the kinetics of mineral-fluid reactions in the form of mineral rate laws into reactive transport numerical codes is a necessary task. The resulting simulations gain reliability as the numerical codes include the kinetics of mineral dissolution/precipitation reactions coupled to the transport equations *(Steefel and Lasaga, 1994; Saaltink et al., 2004)*.

Therefore, we constantly need to improve our knowledge of water-rock/mineral interaction. Within this context, along these years, the kinetics of the following minerals/materials has been studied: smectite, kaolinite and biotite (clays); pyrite, marcasite, galena, chalcopyrite and sphalerite (sulphides); biogenic hydroxyapatite (phosphate); periclase (oxide); calcite, aragonite and dolomite (carbonates), fluorite (halide), gypsum (sulphate) and fly ash, synthetic NaP1 zeolite and C-S-H gel of the Portland cement paste (silicates).

As a participant in these studies, I'm indebted to all the colleagues who, along these years in different degree and from different Institutions, have been leading or cooperating in the numerous undertaken scientific tasks under distinct research projects: Carles Ayora, Josep M. Soler, Jiwchar Ganor, Tony Lasaga, Ian MacInnis, Sharon Nir, Volker Metz, Araceli Garrido, Rafael Pérez, José M. Nieto, Esteban Sanz, Xavier Querol, Natàlia Moreno, Mapi Asta, Patricia Acero, Giovanni De Giudici, Maria L. Rozalén, Javier Huertas, Elodia Musu, Piero Lattanzi, Andrew Gault, Nicolas Marty, Tom Sato, Christophe Tournassat, Marco Boi, José L. Mogollón, Peter Nico, Carl Steefel, Alastair McDowell, Clara Torrentó, Tobias Rötting, Francesco Offeddu, Ion Tiseanu, Manuela Barbieri, Xavier Sànchez, Radostina Atanassova, Ignasi Casanova, Ana Trapote, Rolf Ardvison, Andreas Lüttge, Li Zhang, Josep Oliva, Joan De Pablo, José L. Cortina, Neus Otero, Albert Soler, Jordi Urmeneta, Maria García, Ignasi Queralt, Chiara Cappelli, Maarten Saaltink, Jesús Carrera, Salvador Galí, Pere Mampel, Ramon Vàzquez and Gaby Dávila.

The paper is divided into four sections according to the three topics of investigation aforementioned, ending with a summary of the experimental techniques and methods

NUCLEAR WASTE

Clays (smectite, kaolinite and biotite)

In the 1990s, the public company ENRESA (Spanish Nuclear Waste Agency) in charge for the management of radioactive wastes and the dismantling of nuclear power plants funded investigation projects addressed to safety analysis of the storage of high-level nuclear waste in burial repositories. Characterization of a

palabras clave: Disolución, Precipitación, Cinética, Interacción-Agua Roca.

key words: Dissolution, Precipitation, Kinetics, Water-Rock Interaction.

*corresponding author: **jordi.cama@idaea.csic.es**

multi-barrier system designed to seal the metal canisters containing waste from groundwater interaction was a significant motivation to ensure the necessary levels of safety (Linares, 1993). Ultimately, the main goal was to insure protection to the environment over hundreds of thousands of years.

Due to its osmotic swelling capacity and cation exchange capacity, smectite is capable to impede interaction between the canister and groundwater and retain undesirable cations. However, the durability of the smectite itself under confinement conditions was a key datum that must be taken into consideration. The Cabo de Gata smectite dissolution kinetics was investigated (Cama et al., 2000). The experimentally determined rate law of smectite dissolution was used to model the chemical evolution of the backfilling material in the multi-barrier system designed to storage nuclear waste as was employed in the FEBEX experiment located in the Grimsel area (ENRESA, 1995; Cama and Ayora, 1998).

Use of flow-through experiments was the experimental approach considered appropriate to establish the dissolution rate dependence on the degree of solution saturation state *(Fig. 1)*.

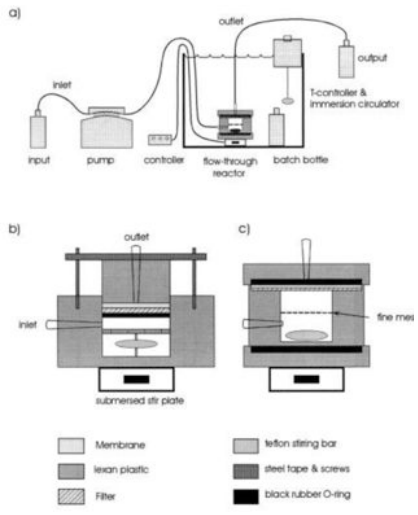

fig 1. General experimental set-up and detailed view of the flow-through reactors; (a) Schematic illustration of the flow-through system; (b) a cell with a Teflon-coated bar mounted on a Lexan pin; (c) a cell with a fine nylon mesh that separates the sample powder and the stir bar. Modified from Cama et al. (2000).

In this type of setup, the mineral powder is placed into the flow reactors, and variation of the aqueous concentration of released cations (e.g., Si, Ca and Mg) with time is monitored *(Fig. 2)*.

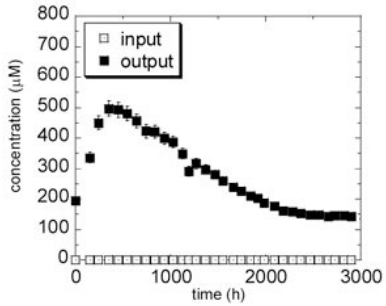

fig 2. Variation in output Si concentration (CSi, out) as a function of time at 25 °C and pH 3 as smectite dissolves. After 2200 h output Si concentration is constant with time (steady-state condition). The smectite steady-state dissolution rate is measured based on output Si concentration (see text). Note that Si input concentration (CSi, inp) is zero

The advantage of this experimental approach is that it allows measurement of dissolution rates under fixed saturation state conditions, pH, temperature, dissolved oxygen, content of catalytic/inhibitory aqueous species, ionic strength, etc. When steady-state conditions are achieved *(Fig. 2)*, the mineral dissolution rate, R (mol m^{-2} s^{-1}), in a well-mixed flow-through experiment is obtained using the following mass balance equation:

$$v_j R = -\frac{q}{A}(C_{j,out} - C_{j,inp})$$

where $C_{j,inp}$ and $C_{j,out}$ are the concentrations of component *j* in the input and output solutions, respectively, νj is the stoichiometry coefficient of j in the dissolution reaction, A is the reactive surface area and q is the fluid volume flux through the system.

In the early studies of smectite dissolution kinetics, SEM (Scanning Electron Microscopy) and the BET (Brunauer-Emmett-Teller) method were used to characterize the mineral changes (particles' morphology and specific surface area, respectively) during smectite dissolution at the microscale.

Recently, Rozalén et al. (2008) studied the pH effect on smectite dissolution over the pH range 1 - 13.5 using both flow-through and batch experiments. Dissolution can be described by a rate law to linking dissolution rates to the concentrations of dissolved protons/hydroxyls. TEM (Transmission Electron Microscopy) confirmed the lack of accessory/companying minerals during smectite dissolution. Marty et al. (2011) have used AFM (Atomic Force Microscopy) to estimate variations in the edge surface area of reacted particles of a synthetic Na-smectite. Accordingly, steady-state rates were normalized to the initial edge surface area. TEM-EDX (Transmission Electron Microscopy and Energy Dispersive X-ray spectrometry) was used to examine variations in chemical composition after smectite reacted.

Weathering of clays occurs in a wide variety of surface and near surface environments. Kaolinite and biotite are clay minerals that are commonly found in host rocks of waste burial sites. The effect that pH, temperature and organic acids exerts on kaolinite dissolution rates, as well as the effect that kaolinite exerts on oxalate degradation were studied by means of flow-through experiments (Cama et al., 2002; Ganor et al., 2001, 2003; Cama and Ganor, 2006). Hence, from the kinetic data obtained, the effects that acid pH and temperature exert on the kaolinite dissolution rate were taken into account in the rate law obtained:

$$Rate = 2\cdot 10^{2}\cdot e^{-22/RT}\cdot\frac{2\cdot 10^{-10}\cdot e^{19/RT}\cdot a_{H^+}}{1+2\cdot 10^{-10}\cdot e^{19/RT}\cdot a_{H^+}} + 5\cdot 10^{7}\cdot e^{-28/RT}\cdot\frac{1.4\cdot 10^{-7}\cdot e^{10/RT}\cdot a_{H^+}}{1+1.4\cdot 10^{-7}\cdot e^{10/RT}\cdot a_{H^+}}$$

where R is the gas constant, T is the temperature (K) and a_{H+} is the proton activity in solution.

The dissolution rates of biotite have been usually obtained from flow-through experiments in which ground powder was used, and the calculated rates were normalised either to total or edge surface area, derived from BET measurements. Optical interferometry is a common tool for measuring the microscopic topography of surfaces. By means of VSI (vertical scanning interferometry) technique, Capelli et al. (2011) are currently attempting to compute biotite dissolution rates by quantifying surface normal retreat of the cleavage (001) surface at pH 1 and 25 - 50 °C. The advantage of these measurements is that allows obtainment of biotite dissolution rates from mineral surface retreat with a nanometric resolution, and thus avoiding the need to normalize the dissolution rates with externally measured surface areas.

Cement/concrete

ENRESA manages the El Cabril disposal facility (Hornachuelos, Andalucia), which is a vault-type surface disposal repository for the storage of the low-and intermediate-level nuclear waste. The concept of this multi-barrier surface disposal system consists of waste packa-

depósito legal: M-38920-2004 • ISSN: 1885-7264

ges (220 L drums) placed inside concrete containers. Mortar is injected into to containers to fill all available space between the drums. The containers are placed inside 24x10x10 m^3 concrete vaults. Our objective is to study the durability of the concrete during all service life of El Cabril disposal facility to guarantee that the properties of this concrete remain unaltered during the operational life of the facility.

C-S-H gel, which constitutes at least 60% of the fully hydrated Portland cement paste, is the main responsible of the durability and barrier properties of cement. Although C-S-H solubility has been studied by many authors, the dissolution kinetics is not known. Flow-through experiments were carried out at room T and under CO_2-free N_2 atmosphere to avoid carbonation. The evolution of pH and Ca and Si concentrations showed that the dissolution of the C-S-H gel is initially incongruent (preferential release of Ca) and evolves to the congruent dissolution of a phase with tobermorite stoichiometry *(Fig. 3)*, which is consistent with the solubility model presented by Kulik and Kersten (2001).

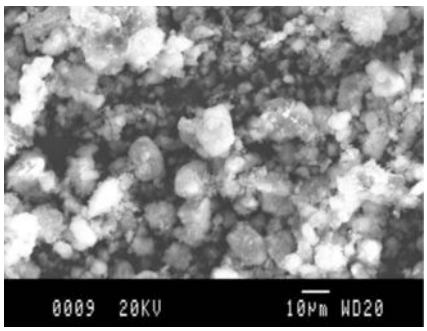

fig 3. SEM image that shows reacted C-S-H gel particles after 60 d at pH between ~12 and ~9.5 and room T under CO_2-free N_2 atmosphere. The solid Ca/Si ratio was analysed by Electron Microprobe suggesting that particles are tobermorite like phase

Trapote et al. (2010) showed that the steady-state dissolution rates of the C-S-H gel normalized to the final BET specific surface area ranged from 10^{-11} to 10^{-10} mol m^{-2} s^{-1}, which are not especially fast, but similar for instance to that of feldspars. These values highlight the necessity of considering C-S-H dissolution kinetics in cases where water flows by advection through mortar or concrete (fast transport; dissolution rate is the limiting factor in C-S-H dissolution).

The authors are currently using the SANS (Small-Angle Neutron Scattering) technique to characterize the microstructure of the C-S-H gel (porous material) at nanometer scale, especially given that the amorphous nature of C-S-H renders diffraction ineffective, and it is most effective in probing features in the 1- to 100-nm size range that defines critical aspects of the C-S-H gel structure. In this technique a coherent beam of neutrons passes through a thin specimen. This fact provokes that a small fraction of the beam may be scattered out of the incident beam direction by a small angle due to interfaces between the microstructural phases. The obtained scattering curve is normalized scattered intensity as a function of scattering angle. These data are analyzed to know microstructural size distribution, pore volume and surface area.

ACID MINE DRAINAGE

Sulphide minerals are present in a large number of natural environments and their weathering is very often an important source of pollution owing to the production of acidity and to the release of metals to soils, surface run-off and groundwaters (Acid Rock Drainage). Similarly, acid mine drainage (AMD) arising mainly from the oxidation of pyrite and other sulfide minerals is a major environmental problem. AMD solutions are characterized by their strong acidity and high concentrations of SO_4^{2-}, Fe, Al and associated trace metals such as Zn, Cu, Pb, Ni, Co and Cd (e.g. Cravotta, 2008). Release of contaminants can persist for decades or centuries after mining has stopped. In contrast to the well-studied mechanism of pyrite dissolution (Rosso and Vaughan, 2006), the dissolution of minor sulphides was not fully investigated. We stressed the need to study the dissolution kinetics of galena, sphalerite, chalcopyrite, arsenopyrite and marcasite in an attempt to propose the respective dissolution rate laws that account for the factors governing the chemical interactions between these sulphides and aqueous solutions (Cama and Acero, 2005; Cama et al., 2005; Asta et al., 2010). Dissolution rate laws accounting for the effects that reactive surface area, aqueous oxygen and protons could exert on the sulphide dissolution reactions were not yet proposed.

Sulphides

In the case of sphalerite dissolution, Acero et al. (2007b) obtained dissolution rates at three different dissolved O_2 concentrations (8.7, 2.1 and 0.2 mg L^{-1}) that were the same within error. This result showed that sphalerite dissolution rate is zeroth order with respect to dissolved O_2 concentration in the pH range 1-3. To obtain the apparent activation energy experimentally, the experiments were carried out at temperatures between 25 and 70 °C whilst maintaining both pH and dissolved O_2 concentration constant (pH 3 and 8.7 mg L^{-1} of dissolved O_2). The slope of the plot of the natural logarithm of the dissolution rates vs. 1000/RT *(Fig. 4)* yields an E_{app} value of ~ 15 kJ mol^{-1}.

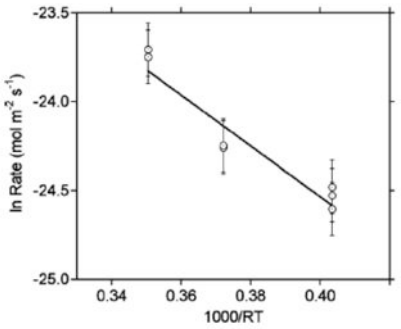

fig 4. Sphalerite dissolution rate dependence on temperature (Arrhenius plot) at pH 3 to calculate the apparent activation energy (E_{app}) of the reaction (modified from Acero et al., 2007b).

On the basis of the low apparent activation energy obtained, sphalerite dissolution rate seems to be transport-controlled. Combination of the reaction order of the sphalerite dissolution rate with respect to H^+, the apparent activation energy (E_{app}) and the rate dissolution constant (k) yielded the following empirical expression for the sphalerite dissolution rate law over the range of acid conditions:

$$R_{\text{sphalerite}} = 10^{-6.49\pm0.02}\, e^{\frac{-14.3\pm1.9}{RT}}\, a_{H^+}^{0.54\pm0.02}$$

where R is the gas constant, T is temperature (K) and a_{H+} is proton activity. XPS examination of the reacted samples confirmed the existence of a surface layer that formed during dissolution and was enriched in S. This layer appears to comprise Zn polysulphides and/or elemental S.

Acero et al. (2007a, 2009) studied the chalcopyrite dissolution kinetics at pH range from 1 to 3 using flow-through experiments; the steady-state dissolution rates of chalcopyrite at this pH were independent of the dissolved oxygen concentrations. The authors observed that iron was released to solution preferentially over copper and sulfur, compared with the stoichiometry of the pristine mineral. Consistently, XPS (X-Ray Photoelectron Spectroscopy) examination of the samples showed that reacted surfaces were enriched in sulfur and copper (relative to iron) compared with the initial, pristine chalcopyrite surface *(Fig. 5)*.

However, this surface layer does not exert any passivating effect on chal-

colpyrite dissolution and the kinetics of the overall process in the long term seems to be surface-controlled.

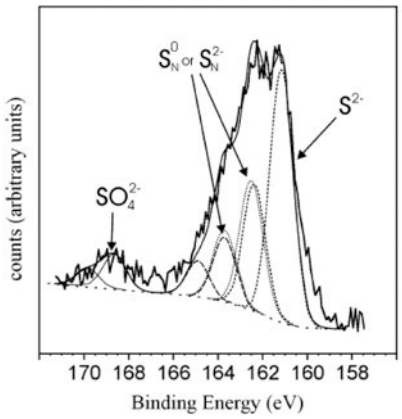

fig 5. Deconvolution of a S2p peak with acceptable signal-to-noise ratio in a representative chalcopyrite sample after the flow-through experiment. The position and interpretation of S-species has been marked (modified from Acero et al., 2009).

Asta et al. (2008) investigated pyrite surface reactivity under AMD conditions, such as pH 1 (HCl), an O_2-saturated atmosphere, and room temperature, including *(1)* ex-situ measurements using VSI and *(2)* solution chemistry measurements using a flow reactor. VSI allowed computation of the reaction rate at a given location of the surface from the surface-normal retreat rate of dissolution. Thus, this absolute rate is calculated independently from any separate determination of surface area (e.g., BET specific area or geometric area). It was concluded that "local" dissolution rates vary widely over mineral surfaces at the short range scale from nano- to millimeter lengths *(Fig. 6)*; *(2)* inferred dissolution rates that are usually based on topographic changes on rather small (micrometer-scale size) surface regions are not necessarily representative of rates under field conditions; and (3) BET surface area and geometric surface area associated with reactive surface area and used to normalize the pyrite dissolution rates yield a variation in rate that ranges from 6.3 x 10^{-11} to 7.2 ± 1.5 x 10^{-9} mol m^{-2} s^{-1}).

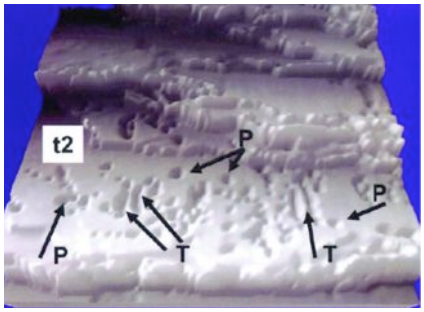

fig 6. 3D image (180 x 90 microns) of the reactive features on a pyrite surface terrace after 21 days (t2) of reaction at pH 1 and room temperature. P indicates rounded boundaries of etch pits; T indicates a train of coalescencent etch pits, and S indicates surface retreat (modified from Asta et al., 2008).

Asta et al. (2010) studied arsenopyrite dissolution kinetics by means of long-term, stirred and non-stirred flow-through experiments in the pH range of 1 to 9 at 25, 50 and 70 °C and at different input dissolved-O_2 concentrations (from 0.2 to 8.7 mg L^{-1}). The rates obtained at 25 °C at acidic pH were DO-dependent, decreasing when the dissolved oxygen concentration is diminished *(Fig. 7)*. At pH lower than 4, aqueous iron, which is mainly in the ferrous form, and arsenic are stoichiometrically released. Sulphur concentrations released were lower than stoichiometrically expected (S/As < 1). XPS and MicroRaman Spectroscopy surface analyses on reacted and unreacted samples showed an enrichment of the reacted arsenopyrite surface in sulphur and arsenic under acidic conditions *(Fig. 8a)*. At pH < 6, aqueous iron is mainly in the ferric form and is depleted as it precipitates as Fe-oxyhydroxide onto arsenopyrite surfaces, yielding Fe/As and Fe/S less than one; between pHs 7 and 9, iron depletion is complete, and sulphur released is more abundant than arsenic released, which is precipitated as As–O phases, as confirmed by MicroRaman spectroscopy *(Fig. 8b)*.

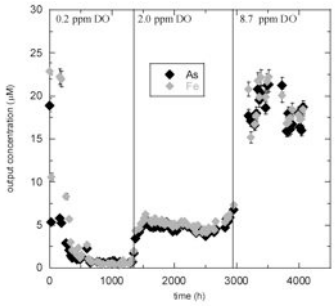

fig 7. Dissolution of arsenopyrite in a long-term flow-through experiment: variation in output concentrations of iron and arsenic as a function of time and dissolved oxygen (DO) at 25 °C and pH 3. Vertical lines delineate the different stages with different input DO concentration at each stage.

TEM examination of the arsenopyrite surfaces reacted at pH 3 at room temperature revealed existence of some amorphopus layers *(Fig. 9)*.

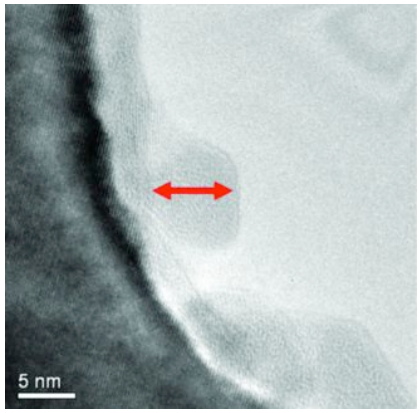

fig 9. TEM image that shows an amorphous layer (arrow) on an arsenopyrite crystalline surface.

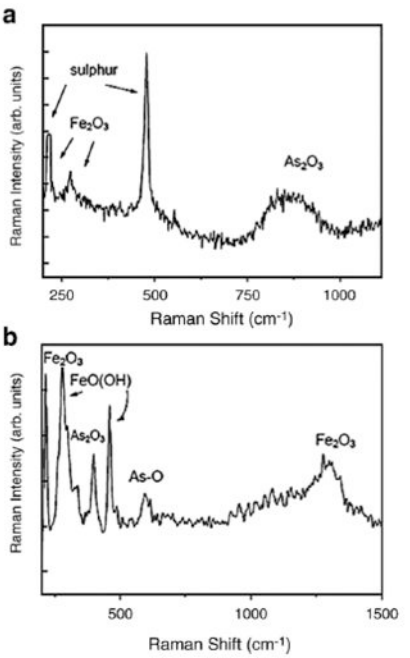

fig 8. MicroRaman spectra of arsenopyrite samples reacted at 8.7 mg L^{-1} DO, 25 °C and pH 3 showing peaks attributed to elemental sulphur, iron oxide and As_2O_3 (a) and pH 7.5 where the peaks are associated with hematite, goethite and traces of claudetite (b). Modified from Asta et al. (2010).

Asta et al. (2010) found out that marcasite oxidative dissolution kinetics at acidic pH resembles that of pyrite and arsenopyrite in long-term experiments.

Cama et al. (2005) studied galena dissolution kinetics by means of in-situ AFM experiments at pH < 3. This experimental approach allows measuring the topographic variation of the surface interacting with the reacting solution with time as the mineral dissolution proceeds. The advantage of this technique is that is non invasive, and hence kinetic measurements do not disturb the reaction mechanism. A systematic section analysis of the surface microtopography variation as dissolution of the {100} cleavage surface occurred was carried out. The AFM-estimated galena dissolution rates were slower than the dissolution rates based on the Pb release probably because of lower reactivity of the area scanned by the AFM probe compared with the entire surface reactivity. The dissolution of galena appeared to be incongruent as aqueous sulphur depletion was observed, resulting in a Pb/S ratio higher than one. It was suggested that through the overall dissolution reaction, a fraction of $H_2S_{(aq)}$ was converted into $H_2S_{(g)}$ as S was detached from the PbS surface, causing the aqueous S deficit. Furthermore, the presence of Fe(III) in solution affects the galena dissolution process by promoting the oxidation reaction of sulphide to sulphate and native sulphur as Fe(III)

depósito legal: M-38920-2004 • ISSN: 1885-7264

reduces to Fe(II). Some of the Pb^{2+} precipitates as $PbSO_4$ (anglesite). However, the main process of removal of S from solution is the S precipitation over the galena substrate *(Fig. 10)*. Also, Acero et al. (2007c) conducted XPS examination of the reacted galena surfaces, showing that reacted surfaces were metal-deficient and S-rich.

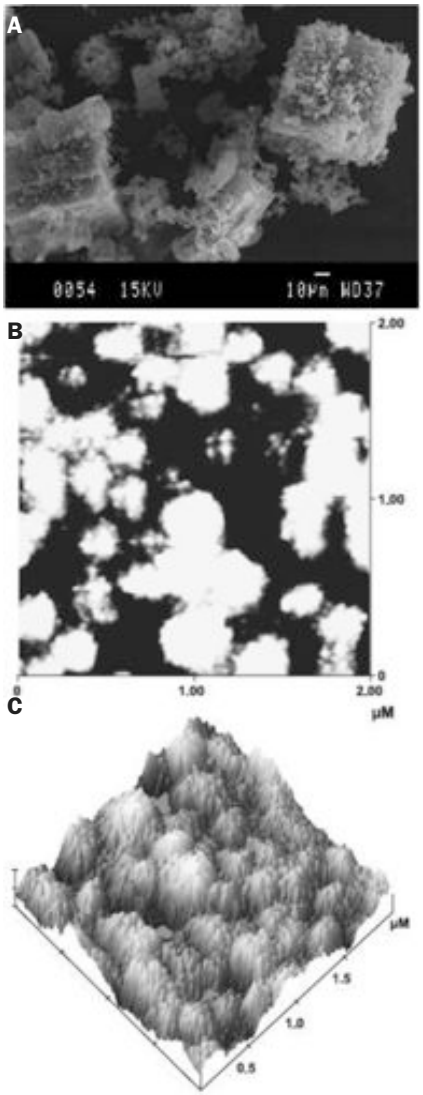

fig 10. SEM photograph showing native sulfur coating all over the galena grains (a). AFM images of galena surface in height mode (upper diagram) and topography mode (lower diagram) after 3.5 h of reaction as 0.01 M $FeCl_3$ was added to the pH 1 (HCl) solution (b) and (c). The surface underwent a tremendous change distinguished by the formation of voluminous protrusions over the galena substrate forming a layer whose thickness grew up to 50 nm in a minute. Modified from Cama et al. (2005).

Therefore, S coating on galena surfaces preventing lead release could in part account for the low Pb concentrations observed in acid mine drainage from pyrite rich ores.

Materials for remediation

Engineering designs for AMD passive treatment systems have been developed since the 1990s (Ziemkiewicz et al., 2003). A basic feature of these systems is that they do not need continuous addition of reactants and only require limited maintenance. Rötting et al. (2008) have proposed the use of dispersed alkaline substrate systems (DAS), which make use of calcite sand mixed with a coarse inert matrix (e.g. wood chips). They have shown that larger Fe(III) and Al concentrations can be treated with this system, but coating of calcite grains by gypsum and clogging by Al-precipitates still occurs. To target the issue of loss of reactivity due to coating of the reactive grains or clogging of porosity, Soler et al. (2008) performed column experiments using calcite sand and synthetic acid solutions that contained only Fe(III)-SO_4^{2-}–H^+ or Fe(III)-Cl^--H^+ as major components. mCT (X-ray microtomography) images of small-diameter clearly showed the precipitation of gypsum directly on the calcite grain surfaces, while Fe-containing phases precipitated further away from those surfaces (towards the center of the pores). Gypsum is always the mineral phase coating the calcite grain surfaces and causing the passivation of the columns *(Fig. 11)*. mXRD (X-ray synchrotron microdiffraction) was tested on a single thin section from a lime column reacted in Fe(III)-SO_4^{2-}-H^+ solution, showing that calcite, gypsum and goethite were the phases identified.

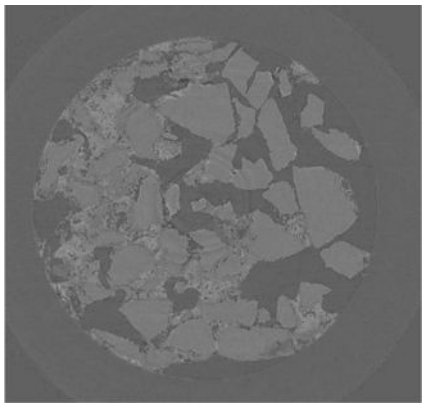

fig 11. X-ray microtomography section of a column in Fe(III)–SO_4^{2-}-H^+ solution. Calcite grains (lighter gray) are coated by gypsum (darker gray). Fe-precipitates are brighter. The formation of preferential pathways for the flow is also evident (non reacted area on the right-hand-side). Column diameter is 1.2 cm. Modified from Soler et al. (2008).

Calcite dissolution in acidic, sulfate-rich waters with divalent metals (Pb, Cu, Zn and Cd among others), promoting metal-sulfate precipitation is a likely scenario *(Fig. 12a)*. It is under such conditions that the calcite dissolution was studied by Queralt et al. (2010). XRF (X-Ray fluorescence spectroscopy) was used to quantify the variation in concentration of the metal-bearing sulfates precipitated on Iceland spar cleavage surface with time in flow-through experiments at room temperature in sulfate solution. After 76 h calcite surface was not yet passivated. Cu precipitation was linear after after 22 h. The precipitation rate of posnjakite was calculated to be $6x10^{-7}$ mol m^{-2} s^{-1} *(Fig. 12b)*.

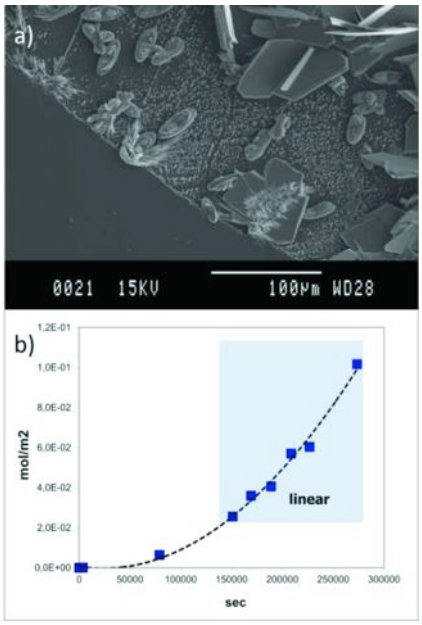

fig 12. SEM image of posnjakite ($Cu_4SO_4(OH)_6{\cdot}H_2O$) precipitates on calcite surface (a). Variation of Cu concentration (mol cm^{-2}) on a cleavage surface of Iceland spar (calcite) with time for 76 h (b).

Caustic magnesia (mainly made up of MgO (periclase) with minor amounts of lime) obtained from calcination of magnesium carbonate was tested as an alternative material to devising passive remediation systems (Cortina et al., 2003). Caustic magnesia reacts with water to form magnesium hydroxide, which dissolves, increasing the pH to values higher than 8.5. Then zinc and lead are mainly precipitated as hydroxides, copper is precipitated as hydroxysulfate, and manganese(II) is oxidized and precipitated as manganese(III) oxides. Thus, metal concentrations as high as 75 mg L^{-1} in the inflowing water are depleted to values below 0.04 mg L^{-1}. Column experiments were designed to measure the reactivity of caustic magnesia under realistic flow conditions. Tracer tests were conducted by adding a known concentration of acetone to the saturating solution to verify uniform flow conditions in the columns and to determine effective transport porosity.

Perez-López et al. (2007) deduced from the flow-through and column experiments, where pyrite oxidation was taking place under saturated conditions and atmospheric oxygen partial pressure, that the addition of fly ash favours

the pyrite sludge dissolution in alkaline conditions and can induce pyrite microencapsulation in a relatively short term. The prevention of pyrite oxidation contributes to the inhibition of acid mine drainage production, becoming a significant advance in the restoration of numerous sources of AMD pollution. Likewise, the column experiments in the paper showed that the fly-ash is an acidity neutralizing material, whose leaching before sludge dissolution attenuates pyrite oxidation by microencapsulation of pyrite grains *(Fig. 13)*.

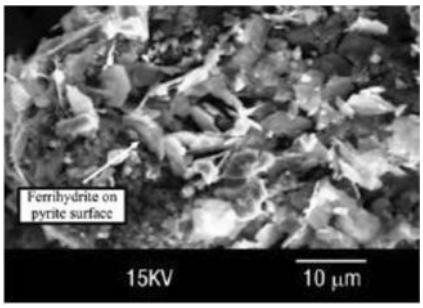

fig 13. SEM photograph showing a pyrite grain coated with Fe-oxyhydroxides (modified from Perez-Lopez et al., 2007).

The PRB is a passive technique which implants a reactive material along the migration path of the polluted aquifer, where groundwater flows and reacts with the material from the barrier, so that, it neutralizes the acidity and retains metals. The PRB fill material is effective if it is enough reactive to reduce the concentrations of the pollutants; it is permeable enough to concentrate the groundwater flow through the barrier; it preserves the permeability and reactivity during a long period of time, and the filling material is available and cheap. An option as reactive material for PRBs is the use of hydroxyapatite. Oliva et al (2010) have investigated the Apatite IITM (from fish bones) removal capacity of Zn, Pb, Mn and Fe using column experiments emulating large scale passive remediation systems. For instance, at pH< 4 the removal capacity of zinc and lead before reaching the breakthrough point (assuming 10% of the input concentration, C/C_o = 0.1) is about 97%. Similar removal capacity was observed at pH> 5. The governing process is the use of phosphate ions, provided by apatite dissolution, to form metal–phosphate minerals *(e.g., hopeite, Fig. 14)*.

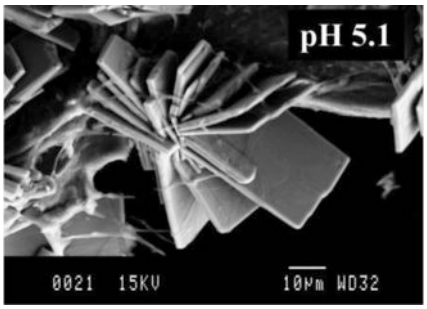

fig 14. SEM image of an aggregate of tabular crystals of hopeite ($Zn_3(PO_4)_2{\cdot}4H_2O$) on apatite II^{TM} substrate reacted at pH 5.1.

Aqueous Zn concentration is in accordance with that expected from an equilibrated solution with respect to hopeite as shown in *Fig. 15*. Upscaling of these results to field scale treatment suggests that a barrier 1-m thick could be operative from 5 to 10 years with water flux as high as 1–10m^3 $m^{-2}y^{-1}$ if the treated-water pH is above pH 4.

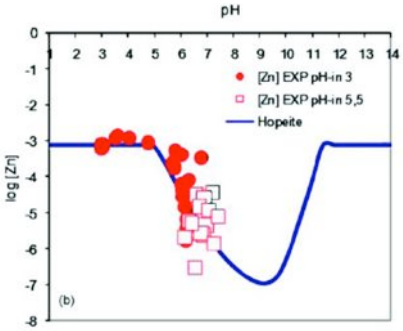

fig 15. Plotted metal concentrations in equilibrium with the phosphorus solid phases were calculated using the speciation code HYDRA (Puigdomènech, 2001). Modified from Oliva et al. (2010).

Fluorite

With the aim to advance in the current knowledge of mineral dissolution kinetics, Cama et al. (2010) decided to investigate the dissolution mechanisms that drive fluorite dissolution at low temperature and acidic pH. Use of VSI and AFM allowed the observation of surfaces that range from tens to hundreds of thousands of square microns. Additionally, to provide theoretical predictions for possible fluorite dissolution mechanisms at the atomic level, a crystal dissolution kinetic model based on the Monte Carlo method was used to simulate the dissolution process on the fluorite (1 1 1) surface.

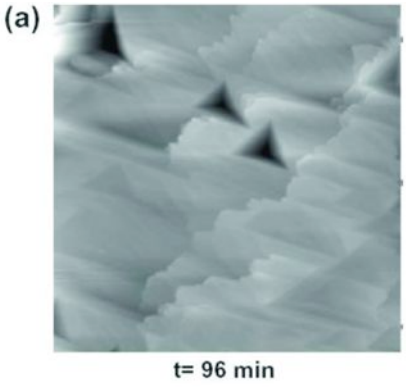

fig 16. In situ AFM topview image (10x10 µm^2) showing a region of the reacted (1 1 1) surface with deep and shallow etch pits at pH 1 for 96 min.

The AFM and VSI observations revealed triangular pits with uniform orientation on the fluorite (1 1 1) surface *(Fig. 16)*, indicating a strong structure control of pit evolution. Monte Carlo simulations adopted the bulk structure of fluorite. The simulations show that in the cleavage (1 1 1) surface that is initially atomically flat formation of triangular etch pits occur *(Fig. 17)*. The modeling investigations suggest that the release of F ions from the surface is preferential relative to Ca ions given the same number of Ca–F connections. The uppermost F layer over the etch pits must be removed so that Ca atoms within the etch pits have F neighbors only from the bottom F layer. This F preferential removal mechanism does not necessitate the removal of the uppermost F layer on the entire terrace. The triangular etch pit generation process will be triggered as long as a local Ca outcrop is formed and followed by Ca removal from the outcrop. The typical triangular pit orientation is attributed to the Ca–Ca arrangements via bridging F neighbors.

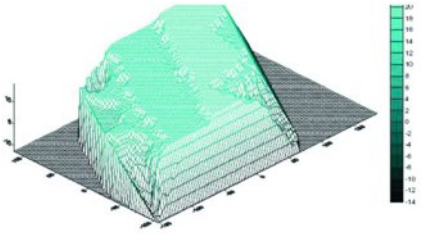

fig 17. Simulated surface topography when steps are incorporated in the (1 1 1) surface. Nucleation of triangular pits and destruction of terrace edges formed as it occurred in the experimentally reacted surfaces (e.g., pH 1). Plot dimensions are numbers of unit cells. Modified from Cama et al. (2010).

GROUNDWATER (DE)NITRIFICATION

Groundwater contamination by nitrate usually originates from anthropogenic sources, mainly as a result of wastewater discharges and the intensive application of fertilizers and animal manure to agricultural land. It is not unusual for groundwater nitrate concentration to exceed the nominal limit of 50 mg L^{-1} set by the 98/83/EC European Union Council Directive. The most significant natural attenuation process is denitrification, i.e. the reduction of nitrate to dinitrogen gas, involving the reduction of nitrate via a chain of microbial reduction reactions to nitrogen gas. Some denitrifiers are autotrophs, obtaining their energy from the oxidation of inorganic species (e.g., pyrite). Although nitrate attenuation, denitrification, mediated by pyrite oxidation is enhanced by bacterial activity (e.g., Thiobacillus Denitrificans), this process (or part of it) may be abiologically controlled (Torrentó and Cama, 2008). The

overall reactions describing the process of denitrification-pyrite oxidation are:
$14\ NO_3^- + 5\ FeS_2 + 4\ H^+ \rightarrow 7\ N_2 + 10\ SO_4^{2-} + 5\ Fe^{2+} + 2\ H_2O$

and

$NO_3^- + 5\ Fe^{2+} + 6\ H^+ \rightarrow {}^1/_2 + 5\ Fe^{3+} + 3\ H_2O$

where denitrification occurs via oxidation of pyrite and Fe(II) and pyrite oxidation is enhanced by the presence of Fe(III).

Torrentó et al. (2010) aimed at experimentally characterize this pyrite-driven denitrification reaction and assessed its feasibility. The process was investigated at different pH and nitrate content by means of long-term flow-through experiments at O_2 partial pressure of 0.003 atm, pH range of 4.5 to 7.5, and NO_3^- concentration from 0.1 to 1.7 mmol L^{-1}. Results showed that as pyrite oxidizes nitrate reduces. At low NO_3^- concentration (0.1 or 0.4 mmol L^{-1}) nitrate reduction is more effective, lasting longer than at high nitrate concentration (1.3 or 1.7 mmol L^{-1}). In the experiments in which nitrate reduction clearly takes place, two stages were distinguished. First, nitrate is reduced to a mixture between nitrite and nitrogen gas, and secondly, nitrate is reduced only to nitrite. Thereafter, nitrate reduction halts.

As regards the flow-through experiments, nitrate reduction occurred in all the non-inoculated and inoculated experiments, but not in a blank experiment. Furthermore, in the T. denitrificans-inoculated experiment, a partial nitrate removal occurred. Subsequently, a complete nitrate removal was achieved and lasted until the end of the experiment (200 d). This suggested a high long-term efficiency of T. denitrificans in nitrate removal using pyrite as the electron donor under the study conditions.

In the flow-through experiments, the pyrite-mass normalized nitrate reduction rate, R_{NO3} (mol g^{-1} s^{-1}) was calculated from the maximum consumption of nitrate according to the expression:

$$R_{NO3} = \frac{q(C_{NO3} - C^0_{NO3})}{m}$$

where q is the flow rate of the solution through the reactor, C_{NO3} and C^0_{NO3} are the concentrations of nitrate in the output and input solutions, respectively, and m is the pyrite mass. In the non-inoculated experiments, computed nitrate reduction rates ranged between 1.62 and 5.42 mmol NO_3-kg_{py}^{-1} d^{-1}. In the inoculated experiment the nitrate reduction rate was 0.54 mmol NO_3-kg_{py}^{-1} d^{-1}, which was lower than in the non-inoculated experiments although nitrate removal efficiency was higher than in the former.

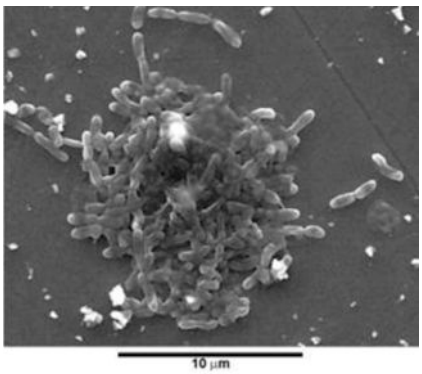

fig 18. SEM image of pyrite surface with an attached micro-colony of cells.

However, little is still known about the involvement of T. denitrificans-like bacteria in the denitrification process *(Fig. 18)*. Batch experiments were performed under anaerobic conditions in a sterilized and anaerobic glove box to determine, clarify and quantify the role of pyrite as an electron donor in the bacterial mediated denitrification process. In most of the pyrite-amended batch experiments nitrite reduction took place rapidly and the final products were N-gaseous compounds (i.e. NO, N_2O or N_2). Furthermore, no changes in the ammonium concentration were detected over time, ruling out dissimilatory nitrate reduction to ammonium.

The results confirmed that these bacteria are able to reduce, at least, nitrate and nitrite. The authors concluded that the addition of pyrite to enhance activity of denitrifying bacteria could be considered for future water management strategies to remove nitrate at the concentrations commonly found in contaminated agricultural groundwater (up to 5 mM, e.g. Otero et al., 2009). However, a drawback of using the pyrite-driven denitrification process as a remediation strategy is at some extent the release of trace metals (e.g. As, Ni) and sulfate as a result of pyrite oxidation.

CO_2 GEOLOGICAL SEQUESTRATION

The trend in global warming observed since the beginning of the industrial revolution is attributed to a great extent to the accumulation of anthropogenic carbon dioxide (CO_2) in the Earth's atmosphere. The capture and storage of CO_2 in geological formations is considered to be one of the most promising approaches to reduce further emissions and to minimize the existing climatic risk until alternatives to fossil fuels become available (IPCC, 2007).

In essence, the geological carbon storage concept consists of injecting supercritical CO_2 into a deep saline aquifer (CO_2 should be in supercritical state to ensure a high density, around 800 kg/m^3, and an efficient use of pore space). This requires pressures nearing 100 bar, which explains why injection needs to be deep. Super-critical CO_2 ($scCO_2$) is less dense and viscous than the reservoir fluid. Therefore, it flows quite easily upwards until it reaches a low permeability, high entry pressure caprock. When $scCO_2$ enters in contact with the formation fluid, dissolution will occur at the interface between the two phases. The interface will display a fingered structure because of gravity, viscosity and capillary instabilities, thus resulting in a relatively large interfacial area between the two phases. In the thin film model of gas exchange, the overall transfer is controlled by the existence of diffusion thin layers on either side of the interface. However, dissolution of CO_2 increases significantly the density of the brine (about 2% depending on salinity), leading to a new gravity instability and the development of heavy fingers of CO_2-saturated brine descending from the buoyant CO_2 plume. This induces a convective flux of dissolved CO_2 to the base of saline aquifers where it can be stably stored. In fact, most mineral reactions will occur in the CO_2 rich brine, which is very acidic, increasing mineral dissolution rates significantly (Riaz et al, 2006).

The coupling of flow and chemical reaction can significantly modify the original porosity, permeability and degree of heterogeneity of the rock (e.g. formation of wormholes). Therefore, there is a need to quantify the mineral reaction rates in the rock, the nature of the secondary minerals precipitating, the volumes of reaction and the consequent changes in porosity.

A test site for a prospective CO_2 reservoir is the Hontomin site (Spain) in which the repository rocks for CO_2 injection are dominantly limestones and dolostones. The injection of CO_2 will cause the formation of CO_2-rich acid brines, which will induce the dissolution of the carbonate minerals. Since the brine contains sulfate, gypsum (or anhydrite at depth) will precipitate, which may cover the surface of the dissolving carbonate causing its passivation. These reactions imply changes in porosity and in the structure of pores in the repository rocks. Therefore, changes in permeability and fluid flow are expected.

García-Rios et al. (2011) and Dávila et al. (2011) are currently carrying out flow-through experiments at room T and atmospheric P_{CO2} with fragments of calcite and dolomite at pH of 1.5 and in-situ AFM experiments with calcite at pH of 2.5. In the flow-through experiments HCl and H_2SO_4 solutions were continually injected into the cells containing the known mass of calcite and only H_2SO_4 solution in the one containing dolomite. In the AFM experiment H_2SO_4 solution was reacting with calcite. All these solutions were equilibrated with respect to gypsum. The evolution of solution composition indicates that the ratio between the volumes of gypsum precipitated and calcite dissolved equals 1.4 ($V_{gyp}/V_{cc\text{-}dis}$ = 1.4), which would translate into a decrease in porosity of the rock matrix. Microscopic examination of the surface of reacted grains suggests that gypsum precipitates heterogeneously upon the surfaces of calcite and dolomite *(Fig.19)*.

fig 19. Gypsum precipitates (white) on calcite (gray) and dolomite (ochre) grains in the flow-through experiments.

Also, an acidic solution (H_2SO_4, pH 2.5) at equilibrium with gypsum was continually injected to react with a known mass of calcite, with a grain size between 1 and 2 mm. Knowing the dissolution rate law for calcite, its surface area (0.5 m^2/g, measured by BET), the volume of solution in the cell and the flow rate, the expected evolution of the solution composition at the outlet of the reaction cell is calculated. Simulations of the experimental results overestimate the dissolution rate of calcite (large increase in pH and Ca concentration). A rapid decrease in sulfate concentration is caused by the precipitation of gypsum, and the model predicts the complete dissolution of calcite.

To refine the model the reactive surface area of calcite was decreased until a match between model and experimental results is achieved. This apparently small reactive surface area likely resides in the effect caused by gypsum precipitating directly on the surfaces of the calcite grains, causing a passivation of the reacting calcite. AFM experiments performed on the calcite cleavage surface reacting with the acidic brine allow studying the mechanism by which gypsum precipitates on the dissolving calcite cleavage surface *(Fig. 20)*.

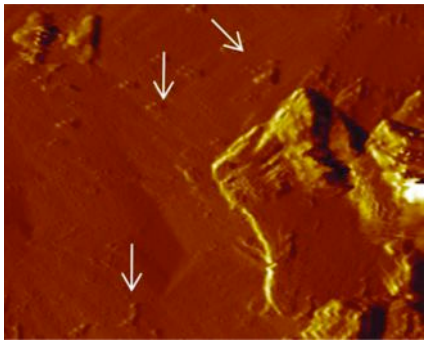

fig 20. AFM image (5x5 μm²) that shows precipitation of gypsum (arrows) on calcite cleavage surface after 25 min. Previous calcite dissolution was characterized by etch pit formation.

These results clearly show that even for such a simple system, reaction rates (including the important passivation effects) have to be studied first in the laboratory. Otherwise, model predictions may be significantly off.

SUMMARY

Macroscopic techniques such as flow-through experiments, batch and column experiments on the basis of aqueous chemistry from reacted minerals' powder have proved to be suitable for (i) quantification of dissolution rates and the effects exerted by environmental variables on them, (ii) to determine the progress of the reactions and (iii) to verify the numerical simulations. The BET method is useful to estimate the specific surface area of the reacted materials. Dissolution rates are often normalized either to the BET specific surface area of non-reacted powder or to that of the reacted one.

The microscopic techniques, SEM-EDX and Electron Microprobe, are used to obtain kinetic data of the reacting surfaces of minerals. Variation of particles' morphology, characterization of dissolution/precipitation features and changes in chemical composition of the solids are readily determined. mXRD and mCT are suitable to determine the mineral composition and variation of pore structure, respectively. At the nanoscale, AFM and VIS are suitable to characterize the evolution of the processes involved in the heterogeneous reactions. In-situ and ex-situ experiments allow measurement of the absolute mineral rates.

XPS is used to quantify the surface stoichiometric ratio as the mineral dissolved. Enrichment of one element compared to the others shows variation of the stoichiometric ratio of the reaction according to the controlling mechanism. XRF is useful to quantify the variation in concentration of metal-precipitates and derive mineral precipitation rates.

Parameterized Monte Carlo simulations prove to be a powerful tool to explore mineral dissolution kinetics. Further modeling should be addressed to precipitation kinetics. Finally, numerical simulations coupling transport with chemical reactions need more experimental data to better predict the evolution of the systems.

ACKNOWLEDGEMENTS

I gratefully acknowledge the technical assistance of Juanjo Cepero, Sandra Toro, Javier Pérez, Óscar Àvila and Josep Elvira from ICTJA, Vanesa Ouro, Mercè Cabanes, Silvia Martínez, Sílvia Rico, Rafael Bartrolí and Alejandro Blanco from IDAEA, Eva Pelegrí, Maite Romero, Toni Padró, Elionor Pelfort, Ana Domínguez, Eva Prats, Javier García, Joan Mendoza, Joaquim Portillo, Jordi Arbiol, Lorenzo Calvo, Ismael Díez, Jordi Díaz and Aranzazu Villuendas from SCT-UB, Rafa Bermúdez from UPC, Emmanuelle Roueff, Boaz Kfir and Ester Shani from BGU, Martin Kunz and Nobumichi Tamura from LBNL and Teddy Craciunescu from NILPRP.

REFERENCIAS

Acero P. Cama J. and Ayora C. (2007a) Kinetics of chalcopyrite dissolution at pH 3. European Journal of Mineralogy 19, 173-182.

Acero P. Cama J. and Ayora C. (2007b) Sphalerite dissolution kinetics in acidic environment. Applied Geochemistry 22, 1872-1883.

Acero P. Cama J. and Ayora C. (2007c) Galena dissolution kinetics in acidic environment. Chemical Geology 245, 219-229.

Acero P. Cama J., Ayora C. and Asta M.P. (2009) Chalcopyrite dissolution rate law from pH 1 to 3. Geologica Acta 7, 389-397.

Asta M.P., Cama J. and Acero P. (2010) Dissolution kinetics of marcasite at acidic pH. European Journal of Mineralogy 22, 49-61.

Asta M.P., Cama J., Acero P., De Giudici G. and Ricci C. (2010) Arsenopyrite dissolution rates in O2-bearing solutions. Chemical Geology 273, 272-285.

Asta M.P., Cama J., Soler J.M., Arvidson R. and Luttge A. (2008) VSI study of pyrite surface reactivity in acidic conditions. American Mineralogist, 93, 508-519.

Cama J. and Acero P. (2005) Dissolution of minor sulphides present in a pyritic sludge at pH 3 and 25 °C. Geologica Acta, 3, 15-26.

Cama J., Acero P., Ayora C. and Lobo A. (2005) Galena surface reactivity at acidic pH and 25 °C based on flow-through and in-situ AFM experiments. Chemical Geology, 214, 309-330.

Cama J. and Ayora C. (1998) Modeling the dissolution behavior in the clayey barrier, Mineralogical Magazine, 62 A, 271-272.

Cama J., Ayora C., Querol X. and Moreno N. (2005) Metal adsorption on clays from pyrite contaminated soil. Journal of Environmental Engineering 131, 1052-1056.

Cama J., Ayora C., Querol X. and Ganor J. (2005) Dissolution kinetics of synthetic zeolite NaP1 and its implication to zeolite treatment of contaminated waters. Environmental Science and Technology 39, 4871-4877.

Cama J. and Ganor J. (2006) The effects of organic acids on the dissolution of silicate minerals: A case study of oxalate catalysis of kaolinite dissolution. Geochimica and Cosmochinica Acta 70, 2191-2209.

Cama J., Ganor J., Ayora C. and Lasaga A. C. (2000) Smectite dissolution kinetics at 80 °C and pH 8.8. Geochimica and Cosmochimica Acta 64, 15: 2701-2717.

Cama J., Metz V. and Ganor J. (2002) The effect of pH and temperature on kaolinite dissolution rate under acidic conditions. Geochimica and Cosmochimica Acta 66, 3913-3926.

Cama J., Zhang L., Soler J.M., De Giudici G., Ardvison R.S. and Luttge A. (2010) Fluorite dissolution in acidic pH: in situ AFM and ex situ VSI experiments and Monte Carlo simulations. Geochimica and Cosmochimica Acta 74, 4298-4311.

Cappelli C., Cama J. and Huertas J.J. (2011) VSI study of biotite dissolution at acidic pH and 25-50 ° C. Geochimica and Cosmochimica Acta, in press.

Cortina J. L., Lagreca I., De Pablo J., Cama J. and Ayora C. (2003) Passive in situ remediation of metal-polluted water with caustic magnesia: evidence from column experiments. Environmental Science and Technology 37, 1971-1977.

Cravotta III, C.A., 2008. Dissolved metals and associated constituents in abandoned coal-mine discharges, Pennsylvania, USA. Part 1: constituent quantities and correlations. Appl. Geochem. 23, 166–202.

Dávila G., García-Rios M. Soler J.M. and Cama J. (2011) Modeling the dissolution of calcite coupled to gypsum precipitation in acid brines. Geophysical Research Abstracts 13, EGU2011-716.

ENRESA (1995) "FEBEX IN SITU TEST" Main report, 179 pp.

Ganor J., Cama J. and Metz V. (2003) Surface protonation data of kaolinite -reevaluation based on dissolution experiments. Journal of Colloid and Interface Science 264, 67-75.

Ganor J., Nir S. and Cama J. (2001) The effect of kaolinite on oxalate (bio)degradation at 25°C and its possible effect on adsorption isotherm measurements. Chemical Geology 177, 431-442.

Garcia, J. E. (2003): Fluid Dynamics of Carbon Dioxide Disposal into Saline Aquifers, Ph. D. thesis, University of California, Berkeley.

García-Rios M., Offeddu G.F., Dávila G., Cama J. and Soler J.M. (2011) Experimental study of calcite dissolution and gypsum precipitation in acid brines. Geophysical Research Abstracts 13, EGU 2011-737.

IPCC (2007) Climate change 2007: synthesis report. In: Pachauri R.K., Reisenger A. (Eds.) Contribution of working Groups I, II and III to the Fourth Intergovernmental Panel on Climate Change. IPCC. Geneva, Switzerland. 104 pp.

Kulik D. A. and Kersten M. (2001) Aqueous solubility diagrams for cementitious waste stabilization systems: II, end-member stoichiometries of ideal calcium silicate hydrates solid solutions. Journal of the American Ceramic Society 84, 3017-3026.

Linares J. (1993) Research on Bentonites as Backfilling Materials in High Level Waste Repositories. ENRESA Technical Publication 01/93, 324 pp.

López R., Cama J., Nieto J. M. and Ayora C. (2007) The iron-coating role on the oxidation kinetics of a pyritic sludge doped with fly ash. Geochimica and Cosmochimica Acta 71, 1921-1934.

Marty N., Cama J., Sato T., Chino D., Villiéras F., Razafitianamaharavo A., Brendlé J., Giffaut E., Soler J.M., Gaucher E.C. and Tournassat C. (2011) Dissolution kinetics of synthetic Na-smectite. An integrated experimental approach. Geochimica and Cosmochimica Acta. In press.

Oliva J., De Pablo J., Cortina J.K., Cama J. and Ayora C. (2010) The Use of Apatite II™ to Remove divalent metal ions Zinc(II); Lead(II); Manganese(II) and Iron(II) from Water in Passive Treatment Systems: Column Experiments. Journal of Hazardous Materials 184, 364-374.

Otero N., Torrentó C., Soler A., Menció A., Mas-Pla J., 2009.Monitoring groundwater nitrate attenuation in a regional system coupling hydrogeology with multi-isotopic methods: the case of Plana de Vic (Osona, Spain). Agr. Ecosyst. Environ. 133, 103–113.

Puigdomènech I. (2001) Chemical Equilibrium Software Hydra and Medusa, Inorganic Chemistry Department, Technology Institute, Stockholm, Sweden.

Queralt I., Offeddu F.G., Cama J., Soler J.M. and Atanassova R. (2010) Energy dispersive X-ray fluorescence (EDXRF) applied to quantify limestone reactivity in acid mine drainage and geological CO_2-sequestration. European Conference on X-ray Spectrometry, EXRS 2010. Session 3. XRS Applications: Earth and environment sciences PS3-33, 309.

Riaz A., Hesse M., Tchelepi H. A. and Orr F. M. (2006) Onset of convection in a gravitationally unstable diffusive boundary layer in porous media. J. Fluid Mech. 548, 87-111.

Rosso K.M. and Vaughan D.J. (2006) Reactivity of sulfide minerals surfaces. Reviews in Mineralogy and geochemistry 61, 557-607.

Rötting T.S., Caraballo M.A., Serrano J.A., Ayora C. and Carrera J. (2008) Field application of calcite Dispersed Alkaline Substrate (calcite-DAS) for passive treatment of acid mine drainage with high Al and metal concentrations. Applied Geochemistry 23, 1660–1674.

Rozalén M. L., Huertas F.J., Brady P.V., Cama J., García-Palma S. and Linares J. (2008) Experimental study of the effect of pH on the kinetics of montmorillonite dissolution at 25 °C. Geochimica and Cosmochimica Acta 72, 4224-4253.

Saaltink M.W., Batlle F., Ayora C., Carrera J. and Olivella S. (2004) RETRASO, a code for modeling reactive transport in saturated and unsaturated porous media. Geologca Acta 2, 235–251.

Soler J.M., Boi M., Mogollón J.L., Cama J., Ayora C., Nico P.S., Tamura N. and Kunz M. (2008) The passivation of calcite in permeable limestone barriers for the treatment of acid mine water. Column experiments with Fe(III)-SO_4-H^+ and Fe(III)-Cl-H^+ solutions at pH 2. Applied Geochemistry 23, 3579-3588.

Steefel C.I. and Lasaga A.C. (1994) A coupled model for transport of multiple chemical species and kinetic precipitation/dissolution reactions with application to flow in single phase hydrothermal systems. Am. J. Sci. 294, 529–592.

Torrentó C. and Cama J. (2008) Kinetics of pyrite oxidation and denitrification. Geochimica and Cosmochimica Acta, 72, A.

Torrentó C., Cama J., Urmeneta J., Otero N. and Soler A. (2010) Denitrification of groundwater with pyrite and Thiobacillus denitrificans. Chemical Geology 278, 80-91.

Trapote A. Cama J., and Soler J.M. (2010) C-S-H gel dissolution kinetics. In Chemical degradation kinetics of cementitious materials. Acta Mineralogica-Petrographica. Abstract Series 6, IMA 2010, 66.

Ziemkiewicz P.F., Skousen J.G., Simmons J. (2003). Long-term performance of passive acid mine drainage treatment systems. Mine Water Environ. 22, 118–129.